Front. Chem. Sci. Eng. 2022, 16(12): 1807−1817
https://doi.org/10.1007/s11705-022-2243-2

RESEARCH ARTICLE

Development of an *in-situ* H_2 reduction and moderate oxidation method for 3,5-dimethylpyridine hydrogenation in trickle bed reactor

Tao Lin[1,2,3,4,5,6,7], **Xiaoxun Ma** (✉)[1,4,5,6,7]

1 School of Chemical Engineering, Northwest University, Xi'an 710069, China
2 Kaili Catalyst & New Materials Co., Ltd. Xi'an 710201, China
3 Shaanxi Key Laboratory of Catalytic Materials and Technology, Xi'an 710201, China
4 Chemical Engineering Research Center of the Ministry of Education (MOE) for Advanced Use Technology of Shanbei Energy, Xi'an 710069, China
5 Shaanxi Research Center of Engineering Technology for Clean Coal Conversion, Xi'an 710069, China
6 Collaborative Innovation Center for Development of Energy and Chemical Industry in Northern Shaanxi, Xi'an 710069, China
7 International Scientific and Technological Cooperation Base of the Ministry of Science and Technology (MOST) for Clean Utilization of Hydrocarbon Resources, Xi'an 710069, China

Abstract The Ru/C catalyst prepared by impregnation method was used for hydrogenation of 3,5-dimethylpyridine in a trickle bed reactor. Under the same reduction conditions (300 °C in H_2), the catalytic activity of the non-*in-situ* reduced Ru/C-n catalyst was higher than that of the *in-situ* reduced Ru/C-y catalyst. Therefore, an *in-situ* H_2 reduction and moderate oxidation method was developed to increase the catalyst activity. Moreover, the influence of oxidation temperature on the developed method was investigated. The catalysts were characterized by Brunauer–Emmett–Teller method, hydrogen temperature programmed reduction H_2-TPR, hydrogen temperature-programmed dispersion (H_2-TPD), X-ray diffraction, energy dispersive spectroscopy, X-ray photoelectron spectroscopy, Raman spectroscopy, O_2 chemisorption and oxygen temperature-programmed dispersion (O_2-TPD) analyses. The results showed that there existed an optimal Ru/RuO_x ratio for the catalyst, and the highest 3,5-dimethylpyridine conversion was obtained for the Ru/C-i1 catalyst prepared by *in-situ* H_2 reduction and moderate oxidation (oxidized at 100 °C). Excessive oxidation (200 °C) resulted in a significant decrease in the Ru/RuO_x ratio of the *in-situ* H_2 reduction and moderate oxidized Ru/C-i2 catalyst, the interaction between RuO_x species and the support changed, and the hard-to-reduce RuO_x species was formed, leading to a significant decrease in catalyst activity. The developed *in-situ* H_2 reduction and moderate oxidation method eliminated the step of the non-*in-situ* reduction of catalyst outside the trickle bed reactor.

Keywords Ru/C catalyst, *in-situ* H_2 reduction and moderate oxidation, *in-situ* reduction, non-*in-situ* reduction, hydrogenation of 3,5-dimethylpyridine

1 Introduction

N-Heterocycles are widely used in many pharmaceuticals, alkaloids, agrochemicals and fine chemicals, and have received extensive attention [1,2]. 3,5-Dimethylpiperidine (DPI) is a very important pesticide intermediate used for the production of tilmicosin, which is mainly prepared by hydrogenation of 3,5-dimethylpyridine (DPY). With the development of fine chemical industry, the application of DPI has greatly expanded [3,4]. In recent years, a new template for the synthesis of SSZ-39 zeolite has put forward higher requirements on the capacity and quality of DPI [5–7]. However, the traditional production process of DPI by kettle reactor (KR) has been unable to meet the market demand for DPI on a large scale. Therefore, a continuous hydrogenation technology with trickle bed reactor (TBR) using Ru/C catalyst was developed. Compared with the conventional KR, the developed TBR has the advantages of higher DPY conversion, stable catalyst performance, milder reaction conditions and large-scale DPY hydrogenation capacity, which has a good industrial application prospect [8]. The TBR is similar to the piston flow reactor with no back mixing (Fig. 1). Back mixing is the main reason for the low catalytic efficiency in the KR,

Received April 10, 2022; accepted October 11, 2022

E-mail: maxym@nwu.edu.cn

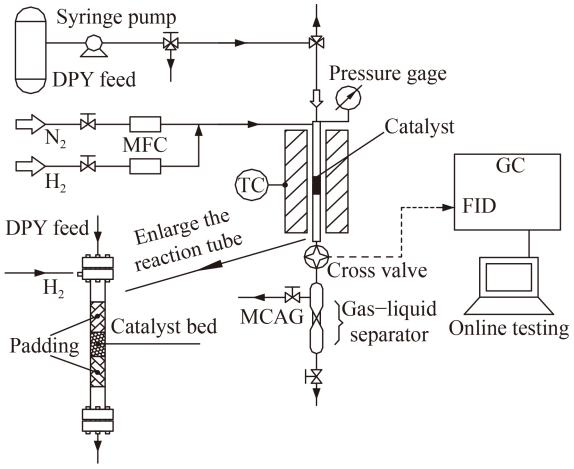

Fig. 1 TBR for DPY hydrogenation.

while mechanical stirring may cause Ru leaching in the KR. The DPY hydrogenation reaction can also be achieved in other continuous hydrogenation reactors but the TBR is a better choice [9]. Although the moving-bed reactor, fluidized bed reactor and microchannel reactor can further improve the mass transfer and heat transfer in this reaction, the requirements of catalyst strength (especially the attrition-strength) are very high, and there may be a risk of easily breaking and blocking the reactor. In addition, the fluidized bed reactor is more expensive, and the application of the three-phase reaction (gas–liquid–solid) in the microchannel reactor is in the early stages. The Ru/C catalyst is the core of the TBR technology, and further study on the structure-activity relationships of this catalyst is an efficient means to prepare catalysts with better catalytic performance.

Ru/C catalyst is a kind of noble metal catalyst with high-cost performance, which is widely used in the field of catalytic hydrogenation with high activity [10,11]. Like other noble metal catalysts, the catalytic property of Ru/C catalyst is affected by the reduction mode, and the reduced Ru/C catalyst tends to be partly oxidized in air. In the KR, the non-*in-situ* reduced Ru/C catalysts are commonly used, which are reduced outside the reactor and then transferred to the KR for the catalytic reaction. For example, Ru/C catalysts used for the hydrogenation of aromatic compounds, sorbitol, and mannitol, are non-*in-situ* reduced by H_2 above 300 °C [12–15]. Due to the high reduction temperature required for the complete reduction of the Ru/C catalyst, it is difficult to achieve *in-situ* reduction in the KR, while *in-situ* reduction is commonly used in the continuous reactors. For example, in ammonia synthesis, *n*-hexane conversion and hydrogenation of levulinic acid, the Ru/C catalysts were reduced *in-situ* in the continuous reactor and then directly used for the reactions [16–20]. The *in-situ* reduction can avoid the oxidation of the reduced Ru/C catalyst when it is exposed to air.

Oxidation or passivation is widely used in the preparation and storage of catalysts, which refers to the formation of a protective oxide layer on the active metal particles by moderate oxidation that prevents their excessive oxidation or sintering when exposed to air [21–23]. Many studies have reported the effects of oxidation conditions and methods on the catalyst activity. Franz et al. [24] studied the impact of catalyst oxidation and reactivation on the catalytic properties of Ni/Al_2O_3 materials in methane dry reforming. Other studies have reported that cobalt-based Fischer–Tropsch catalysts are usually oxidized in diluted O_2 or pure CO_2 [25,26]. Brian et al. [27] studied the effects of oxidation on the synthesis, structure and composition of molybdenum carbide supported platinum catalysts for water–gas shift reaction. Hammache et al. [28] studied the passivation of Ru-promoted Co/alumina catalyst used for Fischer–Tropsch synthesis, and also compared the oxidation effects of different oxidants (CO, CO + H_2 and O_2). Based on the previous studies, it can be concluded that the catalyst oxidation also plays an important role in regulating the performance of catalysts.

In the traditional KR process, the Ru/C catalyst used for DPY hydrogenation is non-*in-situ* reduced. The *in-situ* reduction of Ru/C catalyst is expected in the developed TBR technology, thus eliminating the step of the non-*in-situ* reduction outside the reactor. Few studies have been reported on the effect of oxidation or passivation on Ru/C catalysts used for hydrogenation of pyridine compounds. It is unclear whether Ru/C catalysts for DPY hydrogenation need to be *in-situ* reduced. The effect of moderate oxidation after reduction on the catalytic performance of the Ru/C catalyst has not been reported from KR to TBR. In this paper, the effects of *in-situ* reduction, non-*in-situ* reduction and *in-situ* H_2 reduction and moderate oxidation on the catalytic performance of the Ru/C catalyst were studied, and an *in-situ* H_2 reduction and moderate oxidation method was developed. The catalysts were characterized by Brunauer–Emmett–Teller (BET) method, hydrogen temperature programmed reduction (H_2-TPR), hydrogen temperature-programmed dispersion (H_2-TPD), X-ray diffraction (XRD), energy dispersive spectroscopy (EDS), X-ray photoelectron spectroscopy (XPS), Raman spectroscopy, O_2 chemisorption and O_2-TPD. Based on the characterization results, it is found that the Ru/C-i1 catalyst (*in-situ* reduced and moderately oxidized at 100 °C) is conducive to the improvement of its catalytic performance in the DPY hydrogenation reaction, which may be due to the proper Ru/RuO_x ratio and metal-support interaction on the catalyst.

2 Experimental

2.1 Catalyst preparation

The typical method for the preparation of Ru/C can be

described as follows. First, 10 g catalyst support was impregnated with $RuCl_3 \cdot xH_2O$ (0.811 g, Ru% = 37%) which was dissolved in 16 g hydrochloric acid (1.0 mol·L^{-1}) solution. After 12 h, the excess water was evaporated on a water bath followed by oven drying for 12 h at 120 °C to obtain the unreduced catalyst.

Non-*in-situ* reduced catalyst: the unreduced catalyst was reduced at 300 °C for 2 h in H_2 with a flow rate of 80 mL·min^{-1} in a tube furnace, then cooled down to room temperature in N_2. The obtained catalyst was stored in a dry bottle (exposed in air) for later use, which was marked as Ru/C-n.

In-situ reduced catalyst: the unreduced catalyst was loaded into the TBR for reduction (300 °C for 2 h under H_2 with a flow rate of 80 mL·min^{-1}). After reduction, the catalyst (not exposed to air) was cooled to the reaction temperature, and the hydrogenation reaction was carried out directly. This *in-situ* reduced catalyst was marked as Ru/C-y.

In-situ H_2 reduction and moderate oxidation: the unreduced catalyst was loaded into the TBR for reduction (300 °C for 2 h under H_2 with a flow rate of 80 mL·min^{-1}). After reduction, the catalyst (not exposed to air) was cooled down to room temperature in N_2 flow. The catalyst was moderately oxidized by adding air to N_2 (a total flow rate of 105 mL·min^{-1}) at a low initial O_2 concentration (0.5%, 1% or 2%) for 2 h, then increasing the air flow to slowly increase the O_2 concentration to 3%, 7%, 13% and 21% (pure air) for 0.5 h at each O_2 concentration. The obtained catalyst was marked as Ru/C-i0 (*in-situ* H_2 reduction and moderate oxidation at room temperature). The Ru/C-i0 catalyst was further oxidized in air at 100 °C and 200 °C (for 2 h at a heating rate of 1 °C·min^{-1}), respectively, and the obtained catalysts were marked as Ru/C-i1 and Ru/C-i2 (*in-situ* H_2 reduction and moderate oxidation at 100 °C and 200 °C), respectively.

The carbon support was treated by refluxing in diluted HNO_3 (6%) at 100 °C for 2 h. Then, the mixture was washed until the pH was above 3, and dried to obtain the catalyst support for use. These processing methods allowed carbon support to easily redisperse in polar solvent, which can be attributed to the introduction of oxygenated surface groups [29,30].

2.2 Characterization

The BET surface areas of the catalyst samples were calculated from N_2 adsorption–desorption data acquired on a Gemini VII2390 system (Micromeritics) at liquid N_2 temperature. The specific surface areas were determined according to the BET method, and total pore volumes were obtained from the volume of nitrogen adsorbed at a relative pressure of 0.99. The pore size distribution was acquired from the desorption branches of the isotherms using the Barrett–Joyner–Halenda model.

XRD patterns of the catalysts were recorded on a Miniflex (Rigaku Corporation, Japan) X-ray diffractometer using Ni filtered Cu Kα radiation (λ = 1.5406 Å) with a scan speed of 5°·min^{-1} and a scan range of 10°–60° at 30 kV and 15 mA.

The elements present on the catalysts were analyzed using EDS (Quanta 250 S, FEG).

XPS experiments were carried out with a Thermo Scientific ESCALAB 250Xi instrument. The instrument was equipped with an electron flood and scanning ion gun. All spectra were calibrated to the C 1s binding energy at 284.8 eV.

Raman spectra were recorded on a micro-Raman spectrometer (Thermo DXR2xi) with a 532 nm laser, over the 4000–400 cm^{-1} range.

H_2-TPR, H_2-TPD, O_2 chemisorption and O_2-TPD experiments of as-prepared Ru supported catalysts were carried out using an Auto Chem 2920 instrument. The unreduced Ru/C catalyst was *in-situ* reduced using Auto Chem 2920 instrument (equivalent to Ru/C-y) and then tested.

H_2-TPR was conducted using 100 mg sample. The sample was first flushed by an Ar (99.999%) stream at 150 °C for 180 min to clean its surface, and then cooled down to room temperature, followed by switching to a 10% H_2-Ar mixture as reducing gas (50 mL·min^{-1}) to start the TPR measurement from room temperature to 400 °C.

H_2-TPD was performed using 100 mg of reduced and unreduced catalysts, respectively. The catalyst was heated at a rate of 10 °C·min^{-1} to 300 °C in a flow of 10% H_2-Ar (50 mL·min^{-1}), and maintained at this temperature for 2 h. After cooling down, the catalyst was kept at room temperature for 60 min. Then, the 10% H_2-Ar flow was switched to pure Ar for a period of 30 min. Finally, the catalyst was heated at a rate of 10 °C·min^{-1} and the H_2-TPD curve was recorded.

In O_2 chemisorption and O_2-TPD experiments, the unreduced catalyst sample (100 mg) was pre-reduced in 10% H_2-Ar (50 mL·min^{-1}) at 300 °C for 2 h and flushed subsequently in He flow for 1 h. After cooling down to room temperature, O_2 (10% O_2-He) was injected at regular intervals until there was no more adsorption by catalyst. After O_2 chemisorption, the sample was flushed in He flow until the baseline was stable, then the catalyst was heated at a rate of 10 °C·min^{-1} and the O_2-TPD curve was recorded.

2.3 Catalytic performance tests

Hydrogenation of DPY was tested in TBR (Fig. 1). The reactor system and the analysis process have been described previously [31]. In a typical experiment, 4.0 g catalyst (20–30 mesh) was loaded in the TBR and reduced according to the steps in Section 2.1 (catalyst preparation). N_2 (60 mL·min^{-1}) was used to flush the reaction system for 20 min, then the N_2 flow was

switched to pure H_2. The catalyst bed was heated up to the reaction temperature (1 °C·min^{-1}) and the reaction pressure was 1.0 MPa. DPY was fed by a syringe pump (Lab-alliance Series-III) to the catalyst bed. The mass hour space velocity was 0.5 h^{-1} and the mole ratio of H_2 to DPY was 5:1.

The catalyst samples were stored in a dryer for 12 h or 72 h before catalytic performance evaluation. The products were analyzed by online gas chromatography (GC-2014) equipped with a flame ionization detector, and SE-54 column (30 m × 0.32 mm × 0.5 μm). In these reaction conditions, the selectivity of DPI was close to 100%. The conversion of DPY (X) was calculated on the basis of the following equation:

$$X = \frac{\text{initial concentration of DPY} - \text{final concentration of DPY}}{\text{initial concentration of DPY}} \times 100\%.$$

The conversion of DPY was calculated at 2 h after stable reaction conditions (not the equilibrium conversion).

3 Results and discussion

In order to elucidate the interaction between Ru species and carbon support, various characterization analyses were carried out.

3.1 BET analysis for physical properties

The physico-chemical properties of the samples are listed in Table 1. The specific surface area of the non-*in-situ* reduced Ru/C-n catalyst was found to be 743.6 m^2·g^{-1}. The DPY conversion increased first and then evidently decreased with the rise in oxidation temperature. The Ru species on the catalysts may have a strong interaction with the carbon support at oxidation temperatures of 100 and 200 °C in air atmosphere, which may be the main reason for the slight increase in specific surface area of Ru/C-i1 and Ru/C-i2 catalysts [32,33].

Figure 2 shows the N_2 adsorption–desorption isotherms and pore size distributions of the prepared catalysts. All the samples showed the combination of type I and type IV isotherms according to the IUPAC classification, suggesting the filling phenomenon in mesoporous material [34]. A hysteresis loop of H4 type appeared when the $P{\cdot}P_0^{-1}$ value was around 0.4, further indicating the existence of mesopores and crack pores [33]. In addition, the structures of the carbon support were not destroyed by the increased oxidation temperature. The $P{\cdot}P_0^{-1}$ value of the inflection point did not obviously change with the increase in oxidation temperature, suggesting that pore size of the catalysts was almost independent of the oxidation temperature.

3.2 H_2-TPR analysis for metal-support interaction and H_2-TPD analysis for H_2 desorption

To identify the interaction between Ru species and the carbon support, TPR analysis was performed for the carbon support, unreduced Ru/C, Ru/C-n, Ru/C-y, Ru/C-i0, Ru/C-i1 and Ru/C-i2 catalysts. The results are presented in Fig. 3. TPR analysis is an ideal tool for examining the reducibility and interaction between the metal species and support, and also to obtain information regarding the active state of solid catalysts [35]. As shown in Fig. 3(a), both the carbon support and the Ru/C-y catalyst presented no reduction peaks, indicating that the reduction temperature of 300 °C can fully reduce the Ru/C catalyst. The unreduced Ru/C catalyst consumed a large amount of H_2 in TPR, and the reduction temperature was higher, which may be related to the large amount of Ru^{n+} and Cl species on the catalyst [36]. As shown in Fig. 3(b), two major peaks were observed for Ru/C-n, Ru/C-i1 and Ru/C-i2 catalysts. The reduction peaks observed around 140 °C are reported to be due to the reduction of RuO_x

Table 1 Physico-chemical properties of the samples

Sample	Initial O_2 concentration/%	Storage time/h	S_{BET}[a)]/(m^2·g^{-1})	V_p[b)]/(cm^3·g^{-1})	D_p[c)]/nm	Conversion/%	
						140 °C	100 °C
Ru/C-n	21 (Ari)	12	743.6	0.408	2.93	75.5	5.5
		72				75.7	5.4
Ru/C-y	–	–	–	–	–	65.4	4.2
Ru/C-i0	0.5	12	738.5	0.401	3.08	67.2	4.4
	1	12				67.1	4.4
	2	12				67.5	4.5
	1	72				67.9	4.6
Ru/C-i1	1	12	821.9	0.458	2.89	90.8	8.1
	1	72				90.3	8.1
Ru/C-i2	1	12	804.6	0.423	2.86	33.7	1.5

a) Specific surface area calculated by the BET method; b) total pore volume; c) average pore size based on Barrett–Joyner–Halenda method.

species to Ru^0, or the reduction of Ru(IV) or Ru(III) to Ru (II), corresponding to the easy-to-reduce RuO_x species [37]. The signals between 175 and 300 °C were due to the reduction of Ru(II) to Ru^0, corresponding to the hard-to-reduce RuO_x species [38]. By comparing Ru/C-i0, Ru/C-i1 and Ru/C-i2 catalysts, it can be seen that with the increase in oxidation temperature, the amount of H_2 consumption increased, and the reduction peaks gradually moved to high temperature, indicating that the hard-to-reduce RuO_x species were gradually formed. A large amount of RuO_x was found on the Ru/C-i2 catalyst. The formation of the hard-to-reduce RuO_x species indicated too strong metal-support interaction on the catalyst, which may lead to the decrease in catalyst activity.

H_2-TPD is one of the effective ways to characterize the active sites of the catalyst [39]. The H_2-TPD profiles of the samples are shown in Fig. 4. All catalysts showed a H_2 desorption peak around 80 °C. In the H_2-TPD profile, the height and position of desorption peaks corresponded to the H_2 adsorption capacity and intensity on the catalyst, respectively, indicating that all catalysts had a certain H_2 adsorption capacity. The temperature corresponding to the H_2 desorption peak of Ru/C-y catalyst was the lowest, indicating that its H_2 adsorption intensity was weak. The H_2 desorption peaks of Ru/C-n, Ru/C-i0, Ru/C-i1 and Ru/C-i2 catalysts shifted to the high temperature direction, indicating that the H_2 adsorption ability of the Ru species can be improved by the non-*in-situ* reduction and *in-situ* H_2 reduction and moderate oxidation. As can be seen from the size of the H_2 desorption peaks, Ru/C-i1 and Ru/C-i2 catalysts had relatively large and small H_2 adsorption capacities, respectively. The results indicated that the *in-situ* H_2 reduction and moderate oxidation at an appropriate temperature of 100 °C can effectively improve the H_2 adsorption capacity of Ru/C-i1 catalyst. Oxidation at an excessively high temperature of 200 °C can significantly reduce the H_2 adsorption capacity of Ru/C-i2 catalyst. Therefore, Ru/C-n, Ru/Ci0 and Ru/C-i1 catalysts may have higher catalytic activity than Ru/C-y and Ru/C-i2 catalysts. Different from the Ru/C catalyst used for ammonia synthesis, the reaction temperature of DPY hydrogenation was much lower (around 140 °C), so the H_2 desorption at higher temperatures was not used for comparison [36].

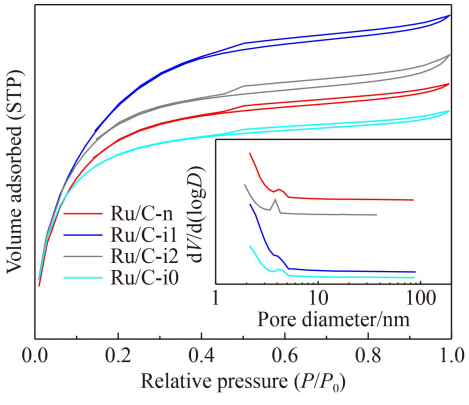

Fig. 2 N_2 adsorption-desorption isotherms and pore size distributions of the Ru/C catalysts.

3.3 XRD analysis for the structure information of catalysts

XRD analysis has been used to reveal the structural information of catalyst nanoclusters together with the carbon supports in many research papers, and is commonly used to obtain information on the active phases present on the catalyst and the average crystallite size [40,41]. The structure of the catalyst determines its properties, so XRD analysis was used to evaluate whether the crystal structures of the catalysts were affected by the oxidation. The XRD patterns of Ru/C-n, Ru/C-i0, Ru/C-i1 and Ru/C-i2 catalysts are given in Fig. 5. All the catalysts presented very similar XRD patterns, which indicated that the crystallinity of the Ru/C catalysts was not significantly affected by the oxidation. There were two broad peaks at 2θ = 25° and 44° for all catalysts, corresponding to (002) and (001) crystal planes from the amorphous graphitic structure of the carbon support (JCPDS-ICDD card No. 41-1487). This indicated that all the samples had amorphous carbon framework [42]. The reduced catalysts were oxidized at different temperatures,

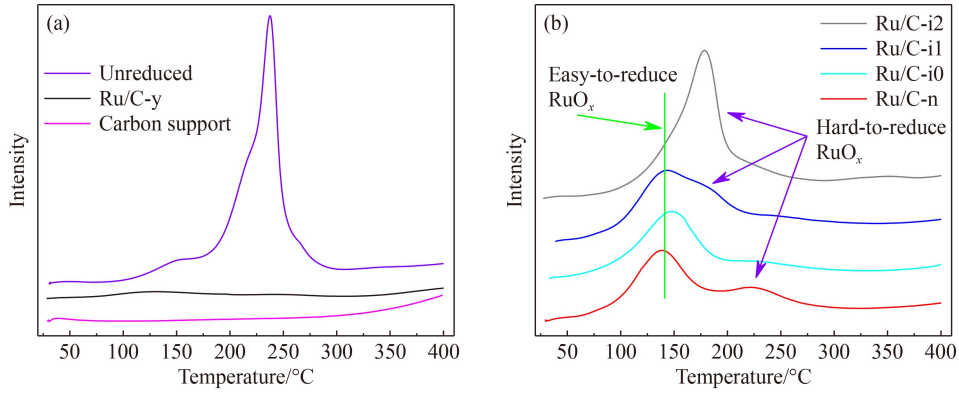

Fig. 3 H_2-TPR profiles of the samples: (a) carbon support, unreduced and Ru/C-y catalyst; (b) Ru/C-n, Ru/C-i0, Ru/C-i1 and Ru/C-i2 catalyst.

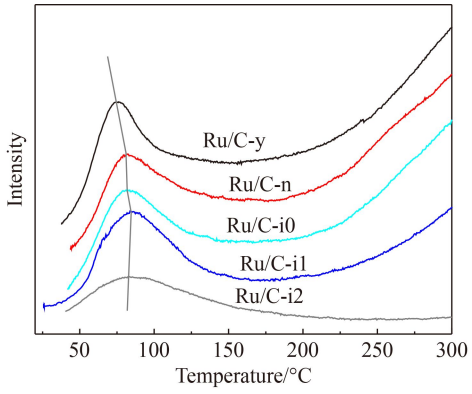

Fig. 4 H_2-TPD profiles of the Ru/C catalysts.

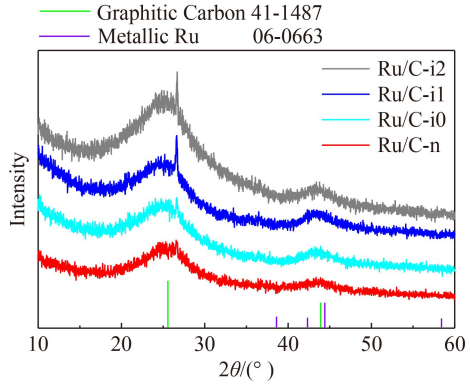

Fig. 5 X-ray diffraction patterns of the Ru/C catalysts.

which may cause the Ru sintering and the formation of RuO_x species on the catalysts. The XRD patterns of all catalysts did not indicate the existence of Ru (JCPDS Card No. 06-0663) and RuO_x species. This implied that the Ru species was well dispersed on the carbon support, even when the oxidation temperature rose up to 200 °C [43]. Therefore, although the XRD profiles of the catalysts were similar, it cannot be determined whether their activities were similar. The difference in the activities of the Ru/C catalysts cannot be obtained from XRD spectra.

3.4 EDS analysis for surface elements of catalysts

The surface elements of the Ru/C catalysts were determined by EDS, and the results are shown in Table 2. There were some impurities on the surface of Ru/C catalysts, in addition to C, O, Cl and Ru elements. The detected Ru content was close to the theoretical value (3%). The results show that the O element increased with the rise in oxidation temperature, indicating that oxidation occurred on the surface of the catalyst.

3.5 XPS analysis for the electronic states

XPS measurements were conducted to analyze the elemental composition and the electronic states of the Ru/C catalysts (Fig. 6). The full XPS spectra of the samples are shown in Fig. 6(a). The peaks located at 200, 285, 460 and 532 eV corresponded to Cl 2p, C 1s+Ru 3d, Ru 3p and O 1s, respectively. This demonstrated the presence of residual Cl element on the samples. The relative contents of C and O on the surface of the catalysts are shown in Fig. 6(a). The relative content of C decreased, while the relative content of O increased on the catalysts with the rise in oxidation temperature, which is in accordance with the EDS results. Figure 6(b) presents the Ru 3d and C1s high-resolution XPS spectra. The Ru 3d peaks around 281 eV were observed in the Ru/C catalysts, which were partially covered by the C1s peaks, probably because the acidic surface functional groups on the carbon caused by HNO_3 can withdraw electron density from Ru atoms [10,12,13]. A weak Ru 3d peak for the Ru/C-i2 catalyst shifted to higher binding energy, which implied that the high oxidation temperature enhanced the electron-deficient state of Ru species [15,44,45]. Therefore, the electronic state of Ru is related to the oxidation temperature.

Table 2 Surface elements of the Ru/C catalysts

Catalyst	Composition and mass fraction of each element/%							
	C	O	Al	Si	S	Cl	Fe	Ru
Ru/C-n	84.31	5.81	0.72	1.76	0.76	1.9	1.63	3.11
Ru/C-i0	84.58	5.88	0.71	1.77	0.75	1.58	1.59	3.14
Ru/C-i1	84.38	6.05	0.71	1.83	0.78	1.55	1.57	3.13
Ru/C-i2	83.46	6.85	0.75	1.79	0.77	1.66	1.55	3.17

The binding energy of the Ru 3p peak was used to further determine the states of Ru species on the Ru/C catalysts (Fig. 6(c)). The Ru 3p peaks were fitted into two peaks at 463.3 and 465.7 eV, which can be attributed to Ru^0 (i.e., metallic Ru) and Ru^{n+} (i.e., RuO_x), respectively [45]. The fitting results including the binding energy and relative content of different peaks are provided in Table 3. The content of Ru^0 species was different on the surface of these catalysts and the amount of metallic Ru was about 72.59%, 88.04%, 86.99% and 59.26% for Ru/C-n, Ru/C-i0, Ru/C-i1 and Ru/C-i2, respectively. The results indicated high electron density of the Ru species and high Ru/RuO_x ratio for the Ru/C-i0 and Ru/C-i1 catalysts. The reason can be attributed to fewer RuO_x species formed on the catalysts due to the *in-situ* H_2 reduction and moderate oxidation (at room temperature and 100 °C, respectively). Harsh oxidation conditions (200 °C) led to deep oxidation of the Ru species on the Ru/C-i2 catalyst, which made the Ru species more electron deficient and significantly decreased the Ru/RuO_x ratio. The electron-rich state and high content of Ru^0 can activate the pyridine rings in the DPY, which may accordingly improve the catalytic activity [45].

3.6 Raman spectroscopic analysis of defects

The Raman spectra (from 0 to 3500 cm^{-1}) for these

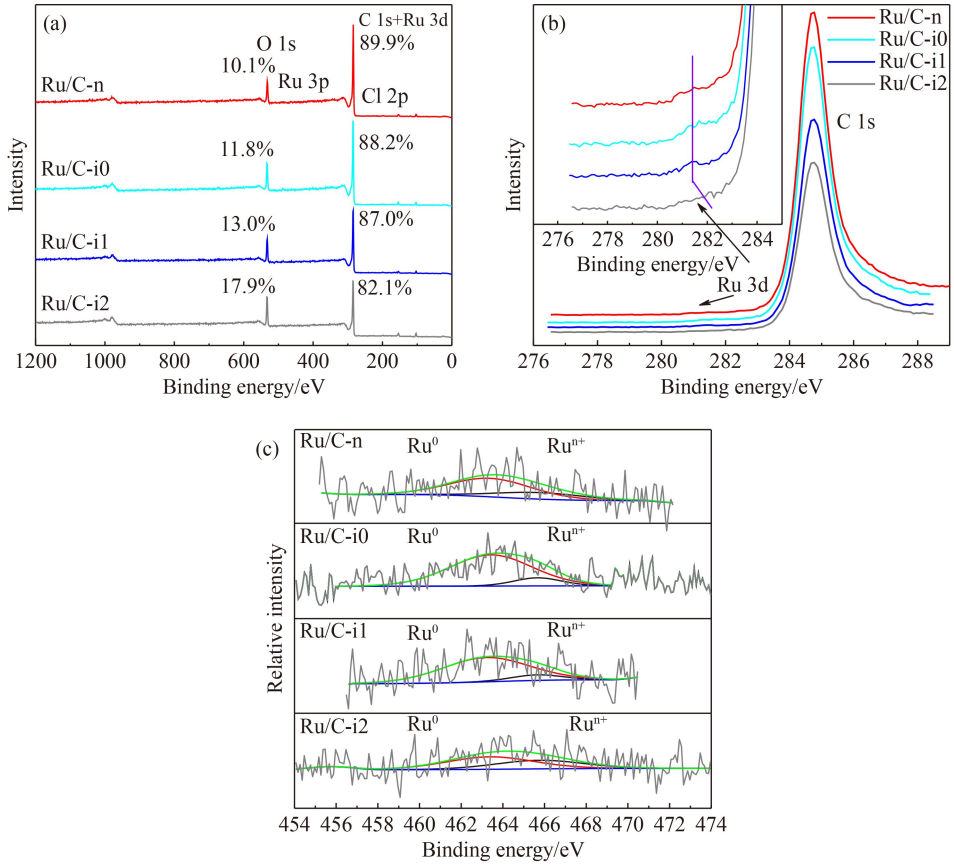

Fig. 6 XPS spectra of Ru/C catalysts: (a) survey spectrum; (b) C 1s + Ru 3d; (c) Ru 3p.

Table 3 Relatively abundance (%) of the components of the Ru 3p spectra

Catalyst	Ru^0		Ru^{n+}		Ru^0/Ru^{n+}
	BE/eV	Area/%	BE/eV	Area/%	
Ru/C-n	463.39	72.59	465.7	27.41	2.65
Ru/C-i0	463.29	88.04	465.7	11.96	7.36
Ru/C-i1	463.42	86.99	465.7	13.01	6.69
Ru/C-i2	463.37	59.26	465.7	40.74	1.45

samples are shown in Fig. 7. Typically, the peaks located at 1340 and 1580 cm^{-1} correspond to defective carbon (D band) and graphitic carbon (G band) structures, respectively [46,47]. The relative number of defects on the catalysts can be obtained by the I_D/I_G (the ratio of peak D band to peak G band). The I_D/I_G ratio of Ru/C-n, Ru/C-i0, Ru/C-i1 and Ru/C-i2 catalysts were 1.13, 1.08, 1.13 and 1.23, respectively. The results showed that with the increase in moderate oxidation temperature, the interaction between Ru species and carbon support was strengthened, and the defects on the catalysts were increased. This is consistent with the BET characterization results.

3.7 O_2 chemisorption and O_2-TPD analyses for RuO_x species

To investigate the RuO_x species on the catalysts, a typical

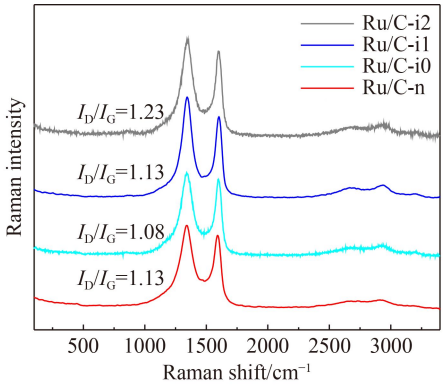

Fig. 7 Raman spectra of the Ru/C catalysts.

O_2 chemisorption experiment was carried out by the pulse method on the Ru/C catalysts (Fig. 8). The *in-situ* reduced Ru/C-i1 catalyst and the non-*in-situ* reduced Ru/C-n catalyst had almost no O_2 consumption in the O_2 chemisorption experiment, indicating that no further oxidation occurred on the Ru/C-n and Ru/C-i1 catalysts (corresponding to the red and blue curves in Fig. 8(a), respectively). The *in-situ* reduced Ru/C-y catalyst was prepared by the unreduced Ru/C catalyst in the chemo radiometer (Auto Chem 2920 instrument) before the text. The Ru/C-y catalyst had O_2 consumption in the O_2 pulse experiment (black curve in Fig. 8(a)). With the increase in

pulse times, the peak area and height of the pulse peaks increased gradually, indicating that the O_2 consumption of the Ru/C-y catalyst decreased until it reached zero [48].

The O_2 consumption experiment of the Ru/C-y catalyst was followed by the O_2-TPD experiment [48]. As can be seen from Fig. 8(b), only a very weak O_2 desorption signal appeared near 70 °C, indicating that the physical adsorption of O_2 on the catalyst was very small and can be ignored. Therefore, the O_2 mainly consumed in O_2 pulses oxidized the Ru^0 species to RuO_x species on the catalyst. The molar ratio of Ru to O on the catalyst can be estimated by the number of Ru on the catalyst and the number of O element consumed in pulses. The calculated O_2 consumption was 0.0902 mL (0.00403 μmol) of the catalyst, so the molar ratio of Ru to O was about 3.69:1 on the catalyst. If the x in RuO_x was 1, the calculated numbers of Ru^0 and Ru^{+2} were 72.9% and 27.1%, respectively. This is consistent with the results obtained by XPS (Ru^0 was 72.6%), indicating that the exposure of the Ru/C-y catalyst to air was basically equivalent to that of Ru/C-n catalyst. The O_2 chemisorption further demonstrated the presence of Ru^0 and RuO_x species on the Ru/C-n catalyst.

3.8 Catalyst performance

The catalytic activity of the catalysts was studied for the hydrogenation of DPY to DPI, and the results are presented in Table 1. The oxygen concentration is an important parameter for oxidation, so the influence of the initial O_2 concentration on the *in-situ* H_2 reduction and moderate oxidation method was first investigated. When the initial O_2 concentration varied from 0.5% to 1.0% and 2.0% (as shown in Table 1), the corresponding DPY conversion did not change significantly (deviation < 1%), indicating that the initial O_2 concentration had little influence on the catalytic activity. Hence, the initial O_2 concentration of 1% was used. The catalysts stored in the dry bottle (exposed in air) may be further oxidized, so the storage time experiment was performed to examine the impact of the different storage times. The catalysts (Ru/C-n, Ru/C-i0 and Ru/C-i1) were stored in the dryer for 12 h and 72 h, respectively, before evaluation. The DPY conversions of Ru/C-n, Ru/C-i0 and Ru/C-i1 catalysts (stored for 72 h) were 75.7%, 67.9% and 90.3%, respectively, which were basically consistent with the results of the 12 h storage (deviation < 1%). Therefore, the effects of oxidation concentration and long-time storage on the DPY conversion were not obvious. The prepared catalysts were relatively stable during the storage process, which is favorable for the application and generalization of the Ru/C catalysts. The industrialized catalysts may have a "shelf life", but the catalysts' activities should not be changed significantly in the short storage term. The activity of the *in-situ* reduced Ru/C-y catalyst was lower than that of the non-*in-situ* reduced Ru/C-n catalyst at the same reaction temperatures (Table 1). Ru/C-i1 catalyst prepared by *in-situ* H_2 reduction and moderate oxidation (100 °C) showed improved activity. DPY conversions of Ru/C-i0, Ru/C-i1 and Ru/C-i2 catalysts increased with the oxidation temperature and then decreased. Ru/C-i1 catalyst showed the highest DPY conversion, while Ru/C-i2 catalyst (oxidized at high temperature of 200 °C) had the lowest activity among these catalysts.

The influence of reaction temperature on the catalysts' activities was investigated (as shown in Fig. 9), and a regular order of the activities was obtained. In the examined temperature range, all the catalysts exhibited a rapid increase in the DPY conversion with the increase in reaction temperature, suggesting that higher reaction temperature was beneficial for the DPY conversion. The order of the DPY conversions at the reaction temperature of 100 °C was as follows: Ru/C-i1 (8.1%) > Ru/C-n (5.5%) > Ru/C-y (4.2%)> Ru/C-i2 (1.5%). The difference in activity with change in the oxidation temperature might be due to the difference in the nature of Ru species on the catalyst [49].

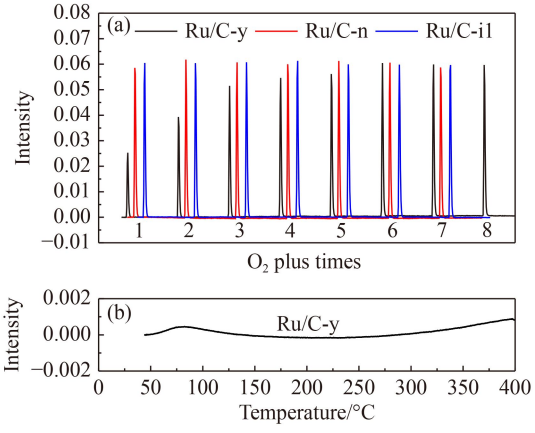

Fig. 8 (a) O_2 chemisorption and (b) O_2-TPD profiles of the Ru/C catalysts.

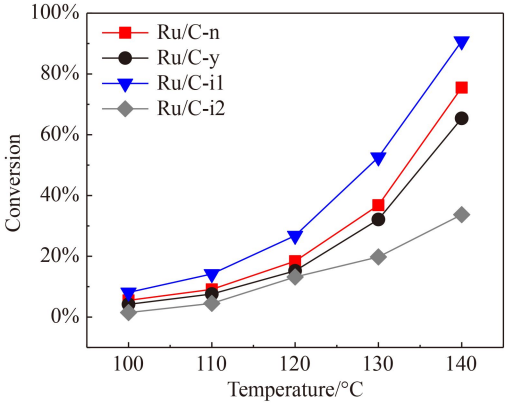

Fig. 9 Effect of reaction temperature on DPY conversion over the Ru/C catalysts.

The developed TBR technique enables the *in-situ* reduction of the Ru/C catalyst, thus eliminating the step of non-*in-situ* reduction outside the reactor. However, the catalytic activity of the *in-situ* reduced Ru/C-y catalyst was lower than that of the non-*in-situ* reduced Ru/C-n catalyst. The reason may be related to the weaker metal-support interaction and hydrogen adsorption capacity compared to other catalysts (Ru/C-n, Ru/C-i0, Ru/C-i1 and Ru/C-i2, in Section 3.2). Ru/C-n catalyst was first reduced and then exposed (oxidized) to air, while Ru/C-i0, Ru/C-i1 and Ru/C-i2 catalysts were first reduced and then moderately oxidized at different temperatures. This suggests that oxidation after H_2 reduction may be beneficial for improving the catalyst activity. Therefore, the *in-situ* H_2 reduction and moderate oxidation method was developed and the influence of the oxidation temperature was investigated. Ru/C-i1 catalyst prepared by *in-situ* H_2 reduction and moderate oxidation method had an optimal Ru/RuO_x ratio (as seen from XPS results in Table 3), strong hydrogen adsorption capacity and strong interaction between Ru species and the carbon support (in Section 3.2). The relatively high Ru/RuO_x ratio on the Ru/C-i1 catalyst can effectively promote the electron transport and activate the pyridine ring, thus accelerating the DPY hydrogenation reaction rate. The strong metal-support interaction can enhance the electron transport and hydrogen adsorption capacity. Hence, the reason for the highest catalytic activity of Ru/C-i1 catalyst may be related to the faster adsorption rate of hydrogen on its active centers, which can provide enough activated hydrogen molecules for the reaction. Furthermore, the *in-situ* H_2 reduction and moderate oxidation (at 100 °C) increased the specific surface area, pore volume (Table 1) and defects (in Section 3.6) of Ru/C-i1 catalyst. These characteristics can promote the diffusion and mass transfer, providing greater surface area and space for the catalytic reaction.

Although the Ru/C-i0 catalyst had higher Ru/RuO_x ratio (Table 3), it exhibited weaker hydrogen adsorption capacity and metal-support interaction (as seen from the results of H_2-TPD and H_2-TPR). The main reason for the lowest activity of Ru/C-i2 catalyst was attributed to its highest oxidation temperature, which caused a large number of Ru^0 to be oxidized to RuO_x. The Ru species was more electron-deficient, which was not conducive to the activation of pyridine ring. Moreover, the amount of adsorbed hydrogen on Ru/C-i2 catalyst was greatly reduced, so the catalytic reaction rate was the lowest. The obtained results of the catalysts' activities and the characterizations can provide guidance for preparing Ru/C catalysts with higher catalytic performance and guarantee their industrial application.

4 Conclusions

The method of *in-situ* H_2 reduction and moderate oxidation was successfully developed, which increased the catalyst activity and eliminated the step of non-*in-situ* reduction of catalyst outside the reactor. At the same reduction temperature (300 °C in H_2), the catalytic activity of the non-*in-situ* reduced Ru/C-n catalyst was higher than that of the *in-situ* reduced Ru/C-y catalyst. This may be due to the interaction of RuO_x species with carbon support on the Ru/C-n catalyst, which improved the adsorption capacity of H_2. The moderate oxidation increased the defects and H_2 adsorption capacity of the catalysts, which had no significant effect on the crystallinity of the catalysts. There existed an optimal Ru/RuO_x ratio for the catalyst, and the Ru/C-i1 catalyst prepared by *in-situ* H_2 reduction and moderate oxidation (100 °C) method showed the highest catalytic activity. Excessive oxidation (200 °C) resulted in a significant decrease in the Ru/RuO_x ratio of the *in-situ* H_2 reduction and moderate oxidation Ru/C-i2 catalyst, and changed the interaction between RuO_x and the support. This resulted in the formation of the hard-to-reduce RuO_x species, leading to a great decrease in catalytic activity.

References

1. Sridharan V, Suryavanshi P A, Menéndez J C. Advances in the chemistry of tetrahydroquinolines. Chemical Reviews, 2011, 111(11): 7157–7259
2. Scott J D, Williams R M. Chemistry and biology of the tetrahydroisoquinoline antitumor antibiotics. Chemical Reviews, 2002, 102(5): 1669–1730
3. Creemer L C, Kirst H A, Shryock T R, Campbell J B, Webb A G. Synthesis, antimicrobial activity and *in vivo* fluorine NMR of a hex fluorinated derivative of tilmicosin. Journal of Antibiotics, 1995, 48(7): 671–675
4. Wan K R, Lin T, Chen J, Li L, Zeng Y K, Zeng L H, Zhang Z X. The preparation method and application of the catalyst used for continuous preparation of 3,5-dimethyl piperidine. Chinese Patent, 201611126557.5, 2016-12-09
5. Beier R C, Creemer L C, Ziprin R L, Nisbet D J. Production and characterization of monoclonal antibodies against the antibiotic tilmicosin. Journal of Agricultural and Food Chemistry, 2005, 53(25): 9679–9688
6. Zones S I, Nakagawa Y, Evans S T, Lee G S. Zeolite SSZ-39. US Patent, 5958370A, 1999-09-28
7. Xu H, Zhang J, Wu Q M, Chen W, Lei C, Zhu Q Y, Han S C, Fei J H, Zheng A M, Zhu L F, Meng X, Maurer S, Dai D, Parvulescu A N, Müller U, Xiao F S. Direct synthesis of aluminosilicate SSZ-39 aeolite using colloidal ailica as a starting source. ACS Applied Materials & Interfaces, 2019, 11(26): 23112–23117
8. Lin T, Ma X X. Development of a new continuous process for the production of 3,5-dimethylpiperidine. Chinese Journal of Chemical Engineering, 2021, 41: 374–383
9. Ranade V V. Trickle bed reactors: reactor engineering & applications. Chemical Industry Press, 2003: 205–215
10. Takasaki M, Motoyama Y, Higashi K, Yoon S H, Mochida I,

Nagashima H. Ruthenium nanoparticles on nano-level-controlled carbon supports as highly effective catalysts for arene hydrogenation. ChemInform, 2007, 39(12): 1524–1533

11. Zhao H, Song H, Zhao J, Yang J, Yan L, Chou L. The reactivity and deactivation mechanism of Ru@C catalyst over hydrogenation of aromatics to cyclohexane derivatives. ChemistrySelect, 2020, 5(14): 4316–4327
12. Wang Y, Rong Z M, Wang Y, Qu J P. Ruthenium nanoparticles loaded on functionalized graphene for liquid-phase hydrogenation of fine chemicals: comparison with carbon nanotube. Journal of Catalysis, 2016, 333: 8–16
13. Wang Y, Rong Z M, Wang Y, Zhang P, Wang Y, Qu J P. Ruthenium nanoparticles loaded on multiwalled carbon nanotubes for liquid-phase hydrogenation of fine chemicals: an exploration of confinement effect. Journal of Catalysis, 2015, 329: 95–106
14. Ban C, Yang S, Kim H, Kim D H. Effect of Cu addition to carbon-supported Ru catalysts on hydrogenation of alginic acid into sugar alcohols. Applied Catalysis A: General, 2019, 578(25): 98–104
15. Ban C, Yang S, Kim H, Kim D H. Catalytic hydrogenation of alginic acid into sugar alcohols over ruthenium supported on nitrogen-doped mesoporous carbons. Catalysis Today, 2020, 352(1): 66–72
16. Liang C H, Wei Z B, Xin Q, Li C. Ammonia synthesis over Ru/C catalysts with different carbon supports promoted by barium and potassium compounds. Applied Catalysis A: General, 2000, 208(1–2): 193–201
17. Upare P P, Lee J M, Hwang D W, Halligudi S B, Hwang Y K, Chang J S. Selective hydrogenation of levulinic acid to γ-valerolactone over carbon-supported noble metal catalysts. Journal of Industrial and Engineering Chemistry, 2011, 17(2): 287–292
18. Song W, Chen Z, Lai W, Rodríguez-Ramos I, Yi X, Weng W, Fang W. Effect of lanthanum promoter on the catalytic performance of levulinic acid hydrogenation over Ru/carbon fiber catalyst. Applied Catalysis A: General, 2017, 540(25): 21–30
19. Ma Y C, Lan G J, Fu W Z, Lai Y, Han W F, Tang H D, Liu H Z, Li Y. Role of surface defects of carbon nanotubes on catalytic performance of barium promoted ruthenium catalyst for ammonia synthesis. Journal of Energy Chemistry, 2020, 29(2): 79–86
20. Guerrero-Ruiz A, Bachiller-Baeza B, Rodríguez-Ramos I. RodríGuez-Ramos I. Catalytic properties of carbon-supported ruthenium catalysts for n-hexane conversion. Applied Catalysis A: General, 1998, 173(2): 231–238
21. Ma Y, Cheng S Q, Wu X D, Ma T X, Liu L P, Jin B F, Liu M H, Liu J B, Ran R, Si Z, Weng D. Improved hydrothermal durability of Cu-SSZ-13 NH_3-SCR catalyst by surface Al modification: affinity and passivation. Journal of Catalysis, 2022, 405: 199–211
22. Tong Q, Cai T, Chen X T, Xu P, Ma Y L, Zhao K, He D. *In-situ* reduction-passivation synthesis of magnetic octahedron accumulated by Fe@Fe_3O_4-C core@complex-shell for the activation of persulfate. Journal of Environmental Chemical Engineering, 2022, 10(4): 108116
23. Birke P, Geyer R, Hoheisel K, Keck M, Pachulski A R, Schödel R. Stability of Ni/SiO_2 catalysts. Chemieingenieurtechnik (Weinheim), 2012, 84(1–2): 165–168
24. Franz R, Tichelaar F D, Uslamin E A, Pidko E A. Dry reforming of methane to test passivation stability of Ni/Al_2O_3 catalysts. Applied Catalysis A, General, 2021, 612(25): 117987
25. Wolf M, Fischer N, Claeys M. Effectiveness of catalyst passivation techniques studied *in situ* with a magnetometer. Catalysis Today, 2016, 275(15): 135–140
26. Fratalocchi L, Groppi G, Visconti C G, Lietti L, Tronconi E. On the passivation of platinum promoted cobalt-based Fischer–Tropsch catalyst. Catalysis Today, 2020, 342(15): 79–87
27. Wyvratt B M, Gaudet J R, Thompson L T. Effects of passivation on synthesis, structure and composition of molybdenum carbide supported platinum water–gas shift catalysts. Journal of Catalysis, 2015, 330: 280–287
28. Hammache S, Goodwin J G Jr, Oukaci R. Passivation of a Co-Ru/γ-Al_2O_3 Fischer–Tropsch catalyst. Catalysis Today, 2002, 71(3): 361–367
29. Moreno-Castilla C, López-Ramón M V, Carrasco-Marín F. Changes in surface chemistry of activated carbons by wet oxidation. Carbon, 2000, 38(14): 1995–2001
30. Collins J, Ngo T, Qu D, Foster M. Spectroscopic investigations of sequential nitric acid treatments on granulated activated carbon: effects of surface oxygen groups on π density. Carbon, 2013, 57: 174–183
31. Lin T, Wan K R, Chen J, Zhang Z X, Zeng Y K, Zeng L H, Gao W. An online device used for evaluating the fixed bed catalyst performance. Chinese patent, 201520609359.9, 2015-08-13
32. Gao P, Wang A, Wang X, Zhang T. Synthesis and catalytic performance of highly ordered Ru-containing mesoporous carbons for hydrogenation of cinnamaldehyde. Catalysis Letters, 2008, 125(3–4): 289–295
33. Su F, Lv L, Lee F Y, Liu T, Cooper A I, Zhao X S. Thermally reduced ruthenium nanoparticles as a highly active heterogeneous catalyst for hydrogenation of monoaromatics. Journal of the American Chemical Society, 2007, 129(46): 14213–14223
34. Lozano-Castelló D, Calo J M, Cazorla-Amorós D, Linares-Solano A. Carbon activation with KOH as explored by temperature programmed techniques, and the effects of hydrogen. Carbon, 2007, 45(13): 2529–2536
35. Veerakumar P, Dhenadhayalan N, Lin K C, Liu S B. Highly stable ruthenium nanoparticles on 3D mesoporous carbon: an excellent opportunity for reduction reactions. Journal of Materials Chemistry A: Materials for Energy and Sustainability, 2015, 3(46): 23448–23457
36. Li Y, Pan C, Han W, Chai H, Liu H. An efficient route for the preparation of activated carbon supported ruthenium catalysts with high performance for ammonia synthesis. Catalysis Today, 2011, 174(1): 97–105
37. Panagiotopoulou P, Vlachos D G. Liquid phase catalytic transfer hydrogenation of furfural over a Ru/C catalyst. ChemSusChem, 2014, 480: 17–24
38. Jae J, Zheng W, Karim A M, Guo W, Lobo R F, Vlachos D G. The role of Ru and RuO_2 in the catalytic transfer hydrogenation of 5-hydroxymethylfurfural for the production of 2,5-dimethylfuran. ChemCatChem, 2014, 6(3): 848–856
39. Li C, Shao Z, Pang M, Williams C, Zhang X F, Liang C H. Carbon nanotubes supported mono- and bimetallic Pt and Ru

catalysts for selective hydrogenation of phenylacetylene. Industrial & Engineering Chemistry Research, 2012, 51(13): 4934–4941

40. Martínez-Prieto L M, Puche M, Cerezo-Navarrete C, Chaudret B. Uniform Ru nanoparticles on N-doped graphene for selective hydrogenation of fatty acids to alcohols. Journal of Catalysis, 2019, 377: 429–437
41. Hossain M A, Phung T K, Rahaman M S, Tulaphol S, Jasinski J B, Sathitsuksanoh N. Catalytic cleavage of the *β*-O-4 aryl ether bonds of lignin model compounds by Ru/C catalyst. Applied Catalysis A: General, 2019, 582(25): 117100
42. Li Z Q, Lu C J, Xia Z P, Zhou Y, Luo Z. X-ray diffraction patterns of graphite and turbostratic carbon. Carbon, 2007, 45(8): 1686–1695
43. Kerdi F, Rass H A, Pinel C, Besson M, Peru G, Leger B, Rio S, Monflier E, Ponchel A. Evaluation of surface properties and pore structure of carbon on the activity of supported Ru catalysts in the aqueous-phase aerobic oxidation of HMF to FDCA. Applied Catalysis A: General, 2015, 506(5): 206–219
44. Zanutelo C, Landers R, Carvalho W A, Cobo A J G. Carbon support treatment effect on Ru/C catalyst performance for benzene partial hydrogenation. Applied Catalysis A: General, 2011, 409–410(15): 174–180
45. Taboada C D, Batista J, Pintar A, Levec J. Preparation, characterization and catalytic properties of carbon nanofiber-supported Pt, Pd, Ru monometallic particles in aqueous-phase reactions. Applied Catalysis B: Environmental, 2009, 89(3–4): 375–382
46. Lin B, Guo Y, Lin J, Ni J, Lin J, Jiang L, Wang Y. Deactivation study of carbon-supported ruthenium catalyst with potassium promoter. Applied Catalysis A: General, 2017, 541(5): 1–7
47. Huang H, Dai Q, Wang X Y. Morphology effect of Ru/CeO_2 catalysts for the catalytic combustion of chlorobenzene. Applied Catalysis B: Environmental, 2014, 158–159: 96–105
48. Rossetti I, Pernicone N, Forni L. Characterisation of Ru/C catalysts for ammonia synthesis by oxygen chemisorption. Applied Catalysis A: General, 2003, 248(1–2): 97–103
49. Michel C, Gallezot P. Why is ruthenium an efficient catalyst for the aqueous-phase hydrogenation of bio-sourced carbonyl compounds? ACS Catalysis, 2015, 5(7): 4130–4132